

# Explanation Bottleneck Models

Shin'ya Yamaguchi<sup>1,2\*</sup> and Kosuke Nishida<sup>1</sup>

<sup>1</sup>NTT, <sup>2</sup>Kyoto University

## Abstract

Recent concept-based interpretable models have succeeded in providing meaningful explanations by pre-defined concept sets. However, the dependency on the pre-defined concepts restricts the application because of the limited number of concepts for explanations. This paper proposes a novel interpretable deep neural network called *explanation bottleneck models* (XBMs). XBMs generate a text explanation from the input without pre-defined concepts and then predict a final task prediction based on the generated explanation by leveraging pre-trained vision-language encoder-decoder models. To achieve both the target task performance and the explanation quality, we train XBMs through the target task loss with the regularization penalizing the explanation decoder via the distillation from the frozen pre-trained decoder. Our experiments, including a comparison to state-of-the-art concept bottleneck models, confirm that XBMs provide accurate and fluent natural language explanations without pre-defined concept sets. Code will be available at <https://github.com/yshinya6/xbm/>.

## 1 Introduction

Although deep learning models can achieve remarkable performance on many applications, they are black-box, i.e., their output predictions are not interpretable for humans. Introducing concept bottleneck models (CBMs, Koh et al. (2020)) is a promising approach to interpreting the output of deep models. In contrast to black-box models that directly predict output labels from input in an end-to-end fashion, CBMs first predict *concept* labels from input and then predict final target class labels from the predicted concepts. Since the predicted concepts represent semantic input ingredients, this two-staged prediction enables users to know the reasons for the final target label predictions and interactively intervene in the decision-making process for critical applications such as healthcare (Chauhan et al. 2023).

However, the existing CBMs depend on the fixed pre-defined concept sets to predict final labels. In other words, they can not provide interpretability to any other than the pre-defined concepts. We argue that this limitation presents a fundamental challenge for CBMs in achieving interpretable deep models. Although recent CBM variants leveraging pre-trained large language models (Yuksekgonul, Wang, and Zou 2023; Oikarinen et al. 2023) enable to express concepts of

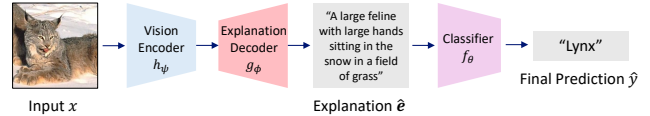


Figure 1: Explanation bottleneck models (XBMs). We propose an interpretable model that generates text explanations for the input embedding with respect to target tasks and then predicts final task labels from the explanations.

arbitrary target classes, the interpretability is still restricted to a fixed and small number of concepts. This is because a large number of concept labels are difficult to learn due to their long-tail distribution and are less interpretable by the limitation of human perception (Ramaswamy et al. 2023). In fact, the prior works restrict the number of concepts by filtering with the similarity between concepts and training images to maintain the performance and interpretability (Oikarinen et al. 2023; Yang et al. 2023). Therefore, as long as they depend on pre-defined concepts, CBMs are restricted in the number of interpretable concepts and are insufficient to explain the output of deep models.

This paper tackles a research problem where we do not assume pre-defined concept sets for constructing interpretable deep neural networks. To this end, we propose a novel family of interpretable models called *explanation bottleneck models* (XBMs), which leverage pre-trained multi-modal encoder-decoder models that can generate text descriptions from input data (e.g., BLIP (Li et al. 2022, 2023)). Leveraging pre-trained multi-modal encoder-decoder enables capturing concepts that actually appeared in the input beyond pre-defined concept sets. Our key idea is to decode concepts as text explanations from input and then predict the final label with a classifier that takes the decoded explanations (Fig. 1). In contrast to CBMs, which make predictions based on pre-defined concepts, XBMs make predictions based on concepts actually appeared in the input data through the decoded explanations and can provide an intuitive interpretation of the final prediction tied to the input. Through end-to-end training, XBMs aim to generate explanations focusing on the textual features for solving the target task.

A major challenge for XBMs is forgetting the text generation capability during training on target tasks. Since target datasets usually lack ground-truth text labels, it is challeng-

\*shinya.yamaguchi@ntt.com

ing to avoid catastrophic forgetting. To generate high-quality explanations, we introduce a training technique called *explanation distillation*, which penalizes the text decoders by the reference explanations generated by frozen pre-trained text decoders. Solving target tasks with explanation distillation enables XBM to decode explanations from input data in natural sentences without corruption.

We conduct experiments to evaluate XBM on multiple datasets by comparing them to existing CBMs and black-box baselines regarding interpretability and target task performance. Our experiments show that XBM can provide a more relevant explanation to input than the pre-defined concepts of existing CBMs while achieving competitive performance to black-box baselines and largely outperforming CBMs in target test accuracy. We also show that training XBM can enhance the multi-modal understanding capability of backbone vision-language models by focusing on the target-related vocabulary. Further, we confirm the reliability and practicality of the XBM’s explanations through the experiments intervening with the random texts and the ground-truth explanations.

## 2 Explanation Bottleneck Models

This section introduces the principle of explanation bottleneck models (XBM). XBM are interpretable deep learning models that predict a final label from the generated explanation text from XBM themselves. Since the predicted final labels are based on the generated explanation of input images, we can naturally interpret the explanation as the reason for the prediction of XBM. Figure 2 illustrates the overview of training an XBM. An XBM consists of a visual encoder  $h_\psi$ , an explanation decoder  $g_\phi$ , and a classifier  $f_\theta$  for predicting final target labels. Among them,  $h_\psi$  and  $g_\phi$  are initialized by an arbitrary pre-trained multi-modal encoder-decoder like BLIP (Li et al. 2022).  $f_\theta$  is a multi-modal classifier built on a transformer that takes the generated explanations as input and conditions the cross-attention layers with image embeddings; this design is inspired by hybrid post-hoc CBMs (Yuksekonul, Wang, and Zou 2023) that uses input embeddings to complement missing concepts not in the predicted concepts. We also confirm the practicality when using a text classifier in Section 3.4. In this section, we mainly describe XBM with a multi-modal classifier. XBM are trained by the target classification loss in an end-to-end manner. Since naïve training leads to collapse in generated text explanation, we avoid the collapse by *explanation distillation*. Explanation distillation penalizes the explanation decoder with a reference text generated from a frozen pre-trained text decoder  $g_p$  to prevent the decoders from forgetting the text generation capability.

### 2.1 Problem Setting

We consider a  $K$ -class image classification task as the target task. We train neural network models  $h_\psi : \mathcal{X} \rightarrow \mathbb{R}^{d_x}$ ,  $g_\phi : \mathbb{R}^{d_x} \rightarrow \mathcal{E}$ , and  $f_\theta : (\mathbb{R}^{d_x}, \mathcal{E}) \rightarrow \mathcal{Y}$  on a labeled target dataset  $\mathcal{D} = \{(x^i, y^i) \in \mathcal{X} \times \mathcal{Y}\}_{i=1}^N$ , where  $\mathcal{X}$ ,  $\mathcal{E}$ , and  $\mathcal{Y}$  are the input, text explanation, and output label spaces, respectively. The text explanation space consists of token sequences of the length  $L$  with token vocabulary  $\mathcal{V}$ , i.e.,  $\mathcal{E} = \mathcal{V}^L$ .  $h_\psi$  is a vision encoder, which embeds an input  $x$  into  $d_x$

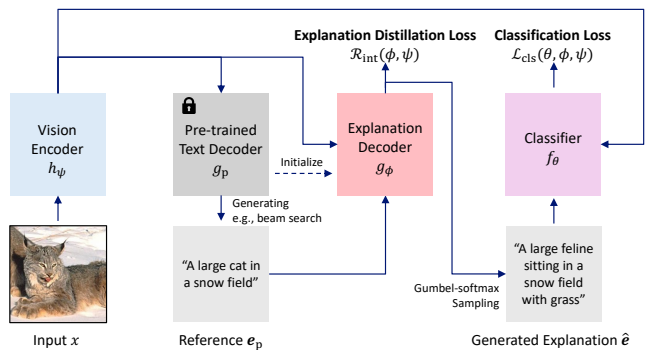


Figure 2: Training of XBM. An XBM is optimized by the target task loss with explanation distillation. Explanation distillation leverages a reference explanation  $e_p$  generated from a pre-trained text decoder  $g_p$  for penalizing the output distribution of an explanation decoder  $g_\phi$  to maintain the interpretable text generation capability of  $g_\phi$ .

dimensional space,  $g_\phi$  is an auto-regressive text decoder that generates a text explanation  $e \in \mathcal{E}$  from an input embedding  $h_\psi(x)$ , and  $f_\theta$  is a classifier that predicts a final target task label  $y$ . We assume that  $h_\psi$  and  $g_\phi$  are initialized by pre-trained multi-modal model’s parameters  $\psi_p$  and  $\phi_p$ , which are pre-trained on large-scale text-image paired datasets with an existing method such as BLIP (Li et al. 2022) and LLaVA (Liu et al. 2023). Note that we do not assume ground truth text explanation set  $\{e^i\}_{i=1}^N$  in  $\mathcal{D}$  for training  $g_\phi$ .

This setting is similar to that of concept bottleneck models (CBMs, Koh et al. (2020)), where a model predicts a final label  $y$  from a set of concepts  $\{c^j \in \mathcal{C}\}_{j=1}^M$  decoded from input  $x$  instead of using  $e$ . The major difference is in the assumption of pre-defined concept sets: our setting does not explicitly specify the words and phrases for the explanations, whereas CBMs explain the model’s output based on the words and phrases in a pre-defined concept set  $\{c^j\}$ .

### 2.2 Objective Function

XBM aim to achieve high target classification accuracy while providing interpretable explanations of the predictions. To this end, XBM solve an optimization problem with a regularization term defined by the following objective function.

$$\min_{\theta, \phi, \psi} \mathcal{L}_{\text{cls}}(\theta, \phi, \psi) + \lambda \mathcal{R}_{\text{int}}(\phi, \psi), \quad (1)$$

$$\mathcal{L}_{\text{cls}}(\theta, \phi, \psi) = \mathbb{E}_{(x, y) \in \mathcal{D}} \ell_{\text{CE}}(f_\theta \circ g_\phi \circ h_\psi(x), y), \quad (2)$$

where  $\mathcal{R}_{\text{int}}(\cdot)$  is a regularization term that guarantees the fluency of the explanations generated from  $g_\phi$ ,  $\lambda$  is a hyperparameter for balancing  $\mathcal{L}_{\text{cls}}$  and  $\mathcal{R}_{\text{int}}$ , and  $\ell_{\text{CE}}$  is cross-entropy loss. Through this objective, the text decoder  $g_\phi$  is trained to focus on the textual features that are useful for minimizing  $\mathcal{L}_{\text{cls}}$  while keeping the interpretability by  $\mathcal{R}_{\text{int}}$ . We found that  $g_\phi$  easily collapses their output without  $\mathcal{R}_{\text{int}}$ . Thus, the design of  $\mathcal{R}_{\text{int}}$  is crucial for training XBM. However, since we often do not have the ground truth explanation sets in a real-world target dataset  $\mathcal{D}$ , we can not directly penalize  $g_\phi$  with supervised losses as  $\mathcal{R}_{\text{int}}$ . To

overcome this challenge, we introduce a distillation-based approach using pre-trained text decoders in the next section.

### 2.3 Explanation Distillation

XBMs utilize pre-trained multi-modal models as the initial parameters of the text (explanation) decoder  $g_\phi$ . As an auto-regressive sequence model, the pre-trained text decoder  $g_p$  can learn a conditional distribution  $q(e|x)$  as

$$q(e|x) = \prod_{l=1}^L q(e_l|x, e_{<l}), \quad (3)$$

where  $L$  is the maximum token length,  $e_l$  is the  $l$ -th token, and  $e_{<l}$  is the text sequence before  $e_l$ . Since  $g_p$  is trained on large-scale text-image pairs,  $q(e|x)$  is expected to be able to generate a token sequence describing important information of various inputs  $x$ .

Our key idea is to leverage  $q(e|x)$  as the reference distribution for maintaining the interpretability of the generated explanation  $\hat{e} \sim p_\phi(e|x)$ , where  $p_\phi(e|x)$  is the model distribution of  $g_\phi$ . If  $p_\phi(e|x)$  and  $q(e|x)$  are sufficiently close, it can be guaranteed that the interpretability of the sequence generated by  $p_\phi(e|x)$  approximate to that by  $q(e|x)$ . Concretely, we compute the KL divergence between  $p_\phi(e|x)$  and  $q(e|x)$  as the regularization term  $\mathcal{R}_{\text{int}}$  in Eq. (1).

$$\begin{aligned} \mathcal{R}_{\text{int}}(\phi, \psi) &= D_{\text{KL}}(q||p_\phi) = \sum_{e \in \mathcal{E}} q(e|x) \log \left( \frac{q(e|x)}{p_\phi(e|x)} \right) \\ &= \mathbb{E}_{e \sim q(e|x)} \log \left( \frac{q(e|x)}{p_\phi(e|x)} \right). \end{aligned} \quad (4)$$

However,  $D_{\text{KL}}(q||p_\phi)$  is computationally intractable because it requires multiple sequential sampling over  $\mathcal{E} = \mathcal{V}^L$  from  $q(e|x)$  and the back-propagation through all sampling processes of  $p_\phi(e_l|x, e_{<l})$ . To approximate Eq. (4), we focus on the connection to knowledge distillation (Hinton, Vinyals, and Dean 2015). That is, minimizing Eq. (4) can be seen as a knowledge distillation from  $g_p$  to  $g_\phi$ . In such a sense, the approximation is

$$\mathcal{R}_{\text{int}}(\phi, \psi) \approx - \sum_{e \in \mathcal{E}} \mathbb{I}_{e=e_p} \log p_\phi(e|x) = - \log p_\phi(e = e_p|x), \quad (5)$$

where  $e_p$  is the sample from  $q(e|x)$  and  $\mathbb{I}$  is the indicator function returning one when  $e$  equals to  $e_p$  or returning zero otherwise; we omit the constant terms from the approximation for the simplicity. As a concrete procedure, we first generate  $e_p$  from  $g_p$  and then penalize the output logits of  $g_\phi$  through the cross-entropy loss for each output token in a next token prediction task. This approximation technique is well-known as sequence-level knowledge distillation (Kim and Rush 2016) in the field of neural machine translation, and it works well in the knowledge distillation of auto-regressive sequence models. Sequence-level knowledge distillation corresponds to matching the modes of  $p$  and  $q$  and omits to transfer the uncertainty represented by the entropy  $H(q)$  (Kim and Rush 2016). Nevertheless, we consider that this is sufficient for XBMs because the goal of XBMs is to provide interpretable explanations for target task predictions, not to replicate the pre-trained models perfectly. We call the regularization with Eq. (5) *explanation distillation*, and introduce it in training XBMs to maintain the text generation capability.

---

### Algorithm 1: Training of XBMs

---

**Require:** Training dataset  $\mathcal{D}$ , vision encoder  $h_\psi$ , text decoder  $g_\phi$ , classifier  $f_\theta$ , pre-trained parameters  $(\phi_p, \theta_p)$ , training batch-size  $B$ , step size  $\eta$ , trade-off parameter  $\lambda$

**Ensure:** Trained models  $(h_\psi, g_\phi, f_\theta)$

```

1: # Initialize parameters
2:  $\phi \leftarrow \phi_p, \psi \leftarrow \psi_p$ 
3: while not converged do
4:    $\{(x^i, y^i)\}_{i=1}^B \sim \mathcal{D}$ 
5:   # Generating reference explanation
6:    $\{e_p^i\}_i^B \leftarrow \{\text{generate}(g_p, h_p(x^i))\}_i^B$ 
7:   # Gumbel-softmax sampling
8:    $\{\hat{e}^i\}_i^B \leftarrow \{\text{g\_sampling}(g_\phi, h_\psi(x^i))\}_i^B$ 
9:   # Computing batch-mean losses
10:   $\mathcal{L}_{\text{cls}}^B \leftarrow \frac{1}{B} \sum_{i=1}^B \ell_{\text{CE}}(f_\theta(h_\psi(x^i), \hat{e}^i), y^i)$ 
11:   $\mathcal{R}_{\text{int}}^B \leftarrow \frac{1}{B} \sum_{i=1}^B \ell_{\text{CE}}(g_\phi \circ h_\psi(x^i), e_p^i)$ 
12:  # Updating parameters via backprop.
13:   $\theta \leftarrow \theta - \eta \nabla_\theta (\mathcal{L}_{\text{cls}}^B + \lambda \mathcal{R}_{\text{int}}^B), \phi \leftarrow \phi - \eta \nabla_\phi (\mathcal{L}_{\text{cls}}^B + \lambda \mathcal{R}_{\text{int}}^B),$ 
    $\psi \leftarrow \psi - \eta \nabla_\psi (\mathcal{L}_{\text{cls}}^B + \lambda \mathcal{R}_{\text{int}}^B)$ 
14: end while

```

---

### 2.4 Algorithm

**Training** We show the training procedure in Algorithm 1. In the training loop, we first generate the reference and predicted explanations  $e_p$  and  $\hat{e}$  by `generate( $\cdot$ )` and `g_sampling( $\cdot$ )`, respectively (line 4 and 5). To approximate the mode of  $q(e|x)$  and ensure the quality as the reference, we generate  $e_p$  from frozen  $g_p$  by beam search following the previous work (Kim and Rush 2016). For sampling  $\hat{e}$ , we introduce the Gumbel-softmax trick (Jang, Gu, and Poole 2017) to retain the computation graph for the end-to-end training with back-propagation. The  $l$ -th token can be approximately sampled by

$$e_l = \text{softmax}((\log(g_\phi(h_\psi(x))) + \mathbf{g})/\tau), \quad (6)$$

where  $\mathbf{g} = \{g_1, \dots, g_{|\mathcal{V}|}\}$  is a vector of length  $|\mathcal{V}|$  where each element is sampled from  $\text{Gumbel}(0, 1)$  and  $\tau$  is the temperature parameter. Intuitively, the temperature  $\tau$  controls the diversity of the token outputs from  $g_\phi$ ; larger  $\tau$  stimulates more diverse outputs. To obtain diverse and accurate tokens for describing input, we apply exponential annealing to the temperature values according to the training steps, i.e.,  $\tau^{(i+1)} = \tau^{(0)} \exp(-r_a i)$ , where  $i$  and  $r_a$  are training step and annealing rate. This allows XBMs to focus on the diversity of the output tokens in the early training steps and on the quality in the later steps. We evaluate this design choice in Appendix E.1. After sampling  $e_p$  and  $\hat{e}$ , we update all trainable parameters according to the objective function Eq. (1).

**Inference** For the inference of test input  $x$ , we generate  $\hat{e}$  by beam search instead of the Gumbel-softmax trick, i.e.,  $\hat{e} \leftarrow \text{generate}(g_\phi, h_\psi(x))$ . Finally, we return the target label prediction  $\hat{y} \leftarrow f_\theta(h_\psi(x), \hat{e})$  and the explanation  $\hat{e}$  to users. Optionally, XBMs provide the other styles of explanation in addition to  $\hat{e}$  (Fig. 3). A *concept phrase*  $c$  is a noun phrase that compose  $\hat{e}$ , which can be extracted by natural language parser automatically (Feng et al. 2022). Similar to the concept outputs of CBMs,  $c$  provides contributions of noun phrases in text explanations for the prediction. For example, if the

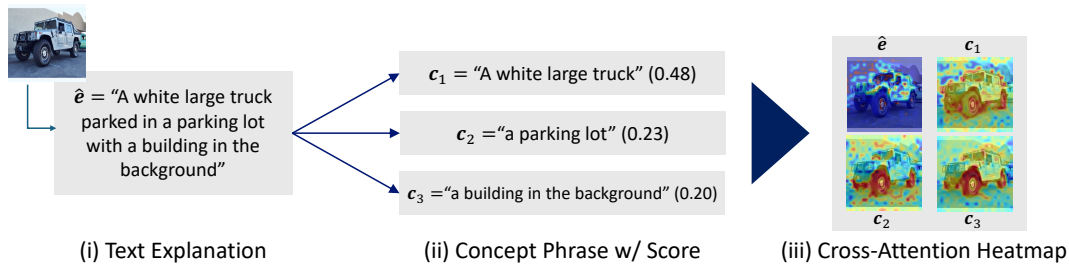


Figure 3: Explanation styles provided by XBMs. XBMs can output (i) text explanation directly generated from the explanation decoder, (ii) concept phrases with self-attention scores in the classifier, and (iii) cross-attention heatmap for the entire text explanation and each concept phrase. Concept phrases are constructed by a natural language parser, and the self-attention scores are computed in a middle layer of the classifier with respect to the  $[\text{CLS}]$  token for each concept phrase. Cross-attention heatmaps are the heatmap visualizations of cross-attention scores between input text tokens and image embedding tokens in the middle layer of the multi-modal classifier (a redder means a higher score).

classifier  $f_\theta$  is implemented with transformer families with attention layers, we can interpret the contribution of  $c$  for the target prediction  $\hat{y}$  via its self-attention scores as in Fig. 3 (ii). Furthermore, we can visualize the cross-attention scores between the text explanations and visual tokens as a heatmap, suggesting what the model perceives as a concept in input data (Fig. 3 (iii)).

### 3 Experiment

We evaluate XBMs on multiple visual classification tasks and pre-training models. We conduct qualitative and quantitative experiments on the explanation outputs of XBMs to evaluate the target performance and the interpretability. We also provide a more detailed analysis, including varying hyperparameters  $\lambda$ ,  $\tau$  and comparing explanation distillation with an alternative regularization loss in Appendix E.

#### 3.1 Setting

**Implementation** Our basic implementation of XBMs is based on BLIP (Li et al. 2022) because of its simplicity; we denote this model as XBM-BLIP. That is, as the visual encoder  $h_\psi$ , we used the ViT-B/32 (Dosovitskiy et al. 2021). For the classifier  $f_\theta$ , we used a BERT-base transformer (Devlin et al. 2019); we input  $h_\psi(x)$  into the cross-attention layers when using a multi-modal classifier inspired by BLIP (Li et al. 2022). We initialized  $\phi$  and  $\psi$  by the BLIP model pre-trained on image captioning tasks in the official repository<sup>1</sup>. We also report the results using larger pre-trained multi-modal models of LLaVA (Liu et al. 2023). We used v1.5 and v1.6 of LLaVA with multiple language model backbones (LLaMA2-7B (Touvron et al. 2023), Vicuna-7B (Chiang et al. 2023), and Mistral-7B (Jiang et al. 2023)); we denote these models as XBM-LLaVA. We provide detailed training settings in Appendix A.

**Baselines** We compare XBMs to black-box and interpretable baselines in performance and interpretability. **Fine-tuned BLIP-ViT** is the black-box baseline, which directly optimizes the visual encoder of BLIP via fine-tuning. **Label-free CBM** (Oikarinen et al. 2023) is a state-of-the-art concept

bottleneck model, which automatically constructs pre-defined concept sets from ConceptNet (Speer, Chin, and Havasi 2017) or GPT-3 (Brown et al. 2020a) and then constructs concept embedding matrix via CLIP vision and text encoder. We used BLIP-ViT as the backbone vision encoder of label-free CBMs. **Frozen BLIP** baselines use frozen BLIP to generate text explanations and predict final labels by a multi-modal  $f_\theta(h_\psi(x), \hat{e})$  or text classifier  $f_\theta(\hat{e})$ . We also show the results of **XBM w/o  $\mathcal{R}_{\text{int}}$** , which updates  $g_\phi$  only on the classification loss Eq. (2).

**Datasets** We used four image datasets for classification tasks in various domains: **Aircraft** (Maji et al. 2013), **Bird** (Welinder et al. 2010), **Car** (Krause et al. 2013), and **ImageNet** (Russakovsky et al. 2015). Aircraft, Bird, and Car are fine-grained image datasets, and ImageNet is a large-scale general image dataset. For datasets other than ImageNet, we randomly split a dataset into 9 : 1 and used the former as the training set and the latter as the validation set. For ImageNet, we set the split ratio 99 : 1 and used the official validation set as the test dataset.

**Evaluation Metrics** We report test accuracy as the target task performance. For the interpretability evaluations, we introduce **CLIP-Score** (Radford et al. 2021; Hessel et al. 2021), which is based on the cosine similarity between image embeddings and text embeddings on CLIP, i.e., higher is better. CLIP-score was originally used to evaluate image captioning based on the relevance of the output captions to the input images. Since it is highly sensitive to the hallucinations in the captions as reported in (Hessel et al. 2021), CLIP-score can be used to assess the factuality of explanations. For XBMs, we measured averaged CLIP-Scores between test inputs and the output explanations. For Label-free CBMs, we measured averaged CLIP-Scores between test inputs and the output concept texts with the binary output of the concept bottleneck layer greater than 0.05; this threshold follows Oikarinen et al. (2023). We also introduce **GPT-2 Perplexity** as a measure of fluency in XBM’s output explanations. In general, perplexity scores on language models are calculated by the averaged cross-entropy of the next token probabilities and thus represent the fluency of the generated texts because the lower perplexity means that the sentence is

<sup>1</sup>model\_base\_caption\_capfilt\_large.pth in <https://github.com/salesforce/BLIP>

Table 1: Performance and Interpretability Evaluation of XBMs on multiple target datasets.

	Aircraft			Bird		
	Test Acc. ( $\uparrow$ )	CLIP-Score ( $\uparrow$ )	GPT-2 Perplexity ( $\downarrow$ )	Test Acc. ( $\uparrow$ )	CLIP-Score ( $\uparrow$ )	GPT-2 Perplexity ( $\downarrow$ )
Fine-tuned BLIP-ViT	77.86	N/A	N/A	83.48	N/A	N/A
Label-free CBM (ConceptNet)	15.37	0.5356	N/A	17.67	0.6025	N/A
Label-free CBM (GPT-3)	44.47	0.6153	N/A	77.74	0.6904	N/A
Frozen BLIP + $f_{\theta}(h_{\psi}(x), \hat{e})$	45.23	0.6824	155.8	68.03	0.7535	173.5
XBM w/o $\mathcal{R}_{\text{int}}$	70.78	0.4730	322.6	61.94	0.5137	431.0
XBM (Ours)	<b>74.09</b>	<b>0.7151</b>	<b>129.8</b>	<b>80.99</b>	<b>0.7942</b>	<b>166.8</b>

	Car			ImageNet		
	Test Acc. ( $\uparrow$ )	CLIP-Score ( $\uparrow$ )	GPT-2 Perplexity ( $\downarrow$ )	Test Acc. ( $\uparrow$ )	CLIP-Score ( $\uparrow$ )	GPT-2 Perplexity ( $\downarrow$ )
Fine-tuned BLIP-ViT	90.08	N/A	N/A	65.21	N/A	N/A
Label-free CBM (ConceptNet)	15.27	0.5561	N/A	60.07	0.6826	N/A
Label-free CBM (GPT-3)	77.91	0.6091	N/A	64.28	0.7026	N/A
Frozen BLIP + $f_{\theta}(h_{\psi}(x), \hat{e})$	80.53	0.6555	168.8	56.04	0.7732	199.5
XBM w/o $\mathcal{R}_{\text{int}}$	86.59	0.4792	415.3	66.58	0.5020	517.1
XBM (Ours)	<b>89.47</b>	<b>0.7173</b>	<b>131.8</b>	<b>67.83</b>	<b>0.7920</b>	<b>122.8</b>

composed of words that are likely to occur probabilistically. Inspired by Chan et al. (2023), we computed perplexity scores of explanations on GPT-2 (Radford et al. 2019). That is, the generated explanations are unbiasedly evaluated by an external language model. GPT-2 perplexity is helpful as a metric of the fluency of explanations because it shows the proximity to the natural text distribution learned by GPT-2. We used open-sourced GPT-2 in huggingface transformers (Wolf et al. 2019) to maintain reproducibility.

### 3.2 Design Evaluation of XBMs

**Quantitative Evaluation** Table 1 demonstrates the quantitative performance and interpretability of XBM-BLIP on the four target datasets. For the target performance, our XBMs outperformed the Label-free CBM baselines and achieved competitive performance with the black-box baseline in the test accuracy. In particular, XBM achieved high performance on datasets where label-free CBM did not perform well (i.e., Aircraft and Car). This can be caused by insufficient pre-defined concepts due to the limited vocabulary in ConceptNet and GPT-3 about describing objects in these datasets, whereas XBMs promote multi-modal understanding by training the explanation decoder to describe arbitrary objects useful for the target dataset with unlimited vocabulary. For the interpretability, XBMs outperformed CBMs in CLIP-Score. This indicates that the explanations from XBMs are more factual to the input images than the concept outputs of CBMs, which are in pre-defined concept sets.



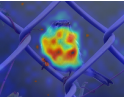
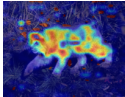
Furthermore, the ablation study in the bottom rows of Table 1 shows that the objective function in Eq. (1) works effectively as we expected. Compared to the frozen BLIP baselines, which simply apply fixed pre-trained BLIP to generate text captions, our XBM significantly improved all of the test accuracy, CLIP-Score, and GPT-2 Perplexity. This suggests that optimizing text decoders with respect to target tasks guides the generated explanation to be informative and target-related for solving the task. We also confirm that the regularization term  $\mathcal{R}_{\text{int}}$  by explanation distillation (Eq. (5)) is crucial to generate meaningful explanation; XBM w/o  $\mathcal{R}_{\text{int}}$

catastrophically degraded CLIP-Score and GPT-2 Perplexity.

**Qualitative Evaluation** Table 2 shows the qualitative studies of explanations generated from XBMs; we also show the other examples in Appendix B. We computed the self-/cross attention scores in the middle of the transformer layers by following Zhang\* et al. (2020). For comparison, we also show the top-3 concept outputs of CBMs and the generated captions of pre-trained BLIP, i.e., the initial states of XBMs. The text explanations of XBMs contain more detailed information than pre-trained BLIP. This is because the target classification loss  $\mathcal{L}_{\text{cls}}$  forces the text decoders to describe target-related visual information to solve the task. Importantly, XBMs without explanation distillation  $\mathcal{R}_{\text{int}}$  generate totally broken explanations, indicating the objective function of XBMs succeed in training the models to focus on the tokens related to the target task without the collapse of explanations. Meanwhile, the concept phrase explanations show the contributions to the final outputs (i.e., self-attention scores) for each noun phrase in the text explanations. In contrast to CBM’s concepts, the concept phrases tend to be aligned with visual features appearing in input images rather than describing input by pre-defined knowledge. This is easy for humans to understand when interpreting the output of the models. Finally, the cross-attention heatmaps intuitively localize where the generated text explanations correspond to the input image spaces. We confirm that the heatmaps concentrate on objects through optimization and facilitate a multi-modal understanding of the image in Section 3.5.

We also analyze the transition of the generated explanations in Fig. 4. We print the text explanation of XBMs and the top-10 word occurrence for all classes and the input class at 0, 20, and 40 epochs. According to the training epoch, the explanations and words progressively focus on detailed and target-related information in images. Concretely, in this example, the XBM is optimized to describe “yellow beak (mouth)”, a key feature of California Gull. These suggest that XBMs can provide interpretable and useful explanations for humans.

Table 2: Qualitative evaluation of explanation outputs.

	Bird (Yellow Bellied Flycatcher)	ImageNet (Lynx)
		
Pre-trained BLIP (Caption)	A bird perched on a wire fence with leaves on the ground and a blurry background.	Cat walking through the grass in the woods at night with it's eyes open.
Label-free CBMs (Top-3 Concept)	olive-colored sides (0.77) green head (0.55) a small, green body (0.52)	feline (0.98) long, sharp claws (0.53) mau (0.17)
XBMs w/o $\mathcal{R}_{\text{int}}$ (Text Explanation)	222222222222 222222222222	when when when when when when when when when when
XBMs (Text Explanation)	A small green and yellow bird perched on a wire fence with leaves on the side.	Furry feline walking in the woods at night with its eyes open and one paw on the ground.
XBMs (Top-3 Concept Phrase)	a small green and yellow bird (0.39) leaves on the side (0.32) a wire fence (0.21)	Furry feline (0.39) one paw on the ground (0.19) the woods (0.17)
XBMs (Cross-Attn. Heatmap)		

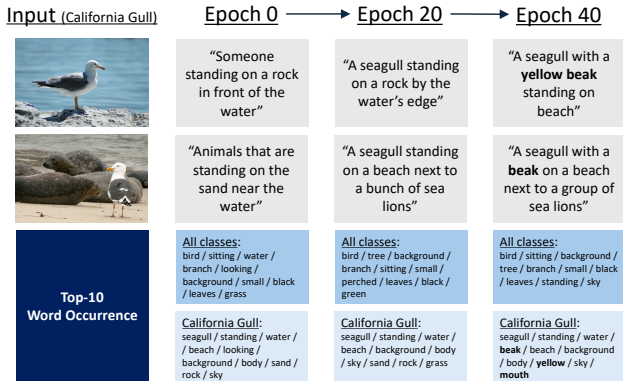


Figure 4: Transition of XBM’s explanation outputs during training (please zoom in).

### 3.3 XBMs with Large Vision-Language Models

Here, we evaluate the scalability and practicality of XBMs by combining them with larger vision-language models than BLIP. Instead of BLIP, we used the LLaVA models with various language model backbones (Liu et al. 2023). Table 3 shows that leveraging the high-performance vision-language model in XBMs yields better performance and interpretability scores, suggesting that the XBM’s objective function can enhance the multi-modal understanding ability even if using the large vision-language models pre-trained on massive image-text pairs. This emphasizes the flexibility of XBM, consisting of arbitrary vision-language models.

### 3.4 XBMs with Text Classifier

Table 3 also evaluates XBMs with a text classifier  $f_{\theta}(\hat{e})$ , which relies only on text information for the final predictions. Although XBM-BLIP with  $f_{\theta}(\hat{e})$  drops the performance from one with a multi-modal classifier  $f_{\theta}(h_{\psi}(x), \hat{e})$ , switching the backbone from BLIP to LLaVA (Liu et al. 2023) resolves

the performance gap. This indicates that more sophisticated vision-language models make XBMs generate informative text explanations, and they can achieve practical performance even when not using input features  $h_{\psi}(x)$ . Appendix C further shows the results on the other datasets.

### 3.5 Evaluations of Cross-Attention Heatmap

The cross-attention heatmap explanation of XBMs visualizes the local input space regions correlated to the text explanation in the classifier. To assess the validity of XBMs on improving multi-modal understanding, we evaluate the generated heatmaps on the ImageNet segmentation task by following Chefer, Gur, and Wolf (2021) and Gandelsman, Efros, and Steinhardt (2024). That is, we generate the heatmaps on the test set of ImageNet Segmentation (Guillaumin, Küttel, and Ferrari 2014) and compute the pixel accuracy, mean IoU (mIoU), and mean average precision (mAP) with the ground truth segmentation masks. Through this evaluation, we can evaluate how heatmaps cover the object of target classes in the pixel spaces. Table 4 shows the results. Compared to the frozen BLIP, XBM-BLIP improved all of the segmentation metrics. This means that the training objective of XBMs encourages the multi-modal understanding of target class objects on the models. In Appendix D, we further compare the XBM’s heat maps with existing attribution methods, such as GradCAM (Selvaraju et al. 2017).

### 3.6 Reliability Evaluation via Human Intervention

CBMs allow the debugging of the model behavior through human intervention in the predicted concepts (Koh et al. 2020). Similarly, we can debug the behavior of XBMs by intervening in the generated explanations. Here, we show examples of an intervention in which all explanations are replaced to check the effect of the explanation quality on the final classification results. At inference, we replace the generated explanations from the explanation decoder with modified explanations. We tested two types of interventions: (i) ran-

Table 3: Evaluation of XBMs with text and multi-modal classifiers built on large vision-language models on ImageNet.

	Text Classifier $f_{\theta}(e)$			Multi-modal Classifier $f_{\theta}(h_{\psi}(x), e)$		
	Test Acc. ( $\uparrow$ )	CLIP-Score ( $\uparrow$ )	GPT-2 Perplexity ( $\downarrow$ )	Test Acc. ( $\uparrow$ )	CLIP-Score ( $\uparrow$ )	GPT-2 Perplexity ( $\downarrow$ )
Frozen BLIP	9.97	0.7732	199.5	56.04	0.7732	199.5
XBM-BLIP	18.26	0.8007	148.1	67.83	0.7920	122.8
Frozen LLaVA-v1.5-LLaMA-7B	64.01	0.7773	236.8	70.21	0.7773	100.8
XBM-LLaVA-v1.5-LLaMA-7B	71.41	0.8008	127.2	72.95	0.7998	82.6
XBM-LLaVA-v1.6-Vicuna-7B	73.73	0.8140	36.74	74.42	0.8037	32.3
XBM-LLaVA-v1.6-Mistral-7B	72.14	0.8037	20.67	74.04	0.8130	21.7

Table 4: Evaluation of cross-attention map of XBMs on ImageNet Segmentation.

	Pixel Acc. ( $\uparrow$ )	mIoU ( $\uparrow$ )	mAP ( $\uparrow$ )
Frozen BLIP + Multi-modal Classifier	78.67	57.90	79.72
XBM-BLIP	80.90	60.80	80.18

Table 5: Evaluation of Intervened XBMs on Bird.

	Test Acc. ( $\uparrow$ )	CLIP-Score ( $\uparrow$ )	GPT-2 Perplexity ( $\downarrow$ )
XBM-BLIP	80.99	0.7942	166.8
Intervened XBM-BLIP (Randomized)	44.42	0.4497	4631.1
Intervened XBM-BLIP (Ground-Truth)	82.21	0.8179	104.5

domized and (ii) ground-truth explanations. For randomized explanation, we used a token sequence uniformly sampled from the vocabulary space for the length of the originally generated explanation. For ground-truth explanation, we used the extended annotation set for Bird proposed by Reed et al. (2016). Table 5 shows the performance of the intervened XBM-BLIP models. The intervened explanations with randomized explanations significantly degraded the performance of XBM-BLIP, indicating that the generated explanations are essential to achieving high performance. In contrast, the intervention with ground-truth explanations largely improved the performance. This suggests that higher-quality explanations can yield higher performance, and intervening with human explanations is helpful for XBMs to improve their performance. In other words, the final prediction of XBMs largely depends on the content of the generated explanation  $\hat{e}$ , indicating that  $\hat{e}$  is a reliable explanation for the final prediction. To conclude, these results support the debuggability of XBMs and the reliability of the generated explanations.

## 4 Related Work

The main research directions of the interpretability of black-box deep neural networks are briefly divided into attribution-based and concept-based methods. Attribution-based methods such as CAM (Zhou et al. 2016) and GradCAM (Selvaraju et al. 2017) generate a localization map representing important regions for the model predictions for specific classes. However, since the maps generated by attribution-based methods do not have information other than that they responded to the predictions, they are less interpretable regarding what semantic input features contribute to the output. In contrast to these methods, our XBMs can generate semantically interpretable heatmaps via cross-attention between image and text explanations, which can be decomposed at the level of noun phrases.

On the other hand, concept-based methods such as TCAV (Kim et al. 2018) and CBMs (Koh et al. 2020) compute contribution scores for pre-defined concepts on intermediate

outputs of models. Among them, CBMs are highly relevant to our XBMs since both have interpretable intermediate layers in models. CBMs predict concept labels and then predict final class labels from the predicted concepts. The original CBMs have the challenge of requiring human annotations of concept labels (Zarlenga et al. 2022; Moayeri et al. 2023; Xu et al. 2024). Post-hoc CBMs (Yuksekgonul, Wang, and Zou 2023) and Label-free CBMs (Oikarinen et al. 2023) addressed this challenge by automatically collecting concepts corresponding to target task labels by querying large language models (e.g., GPT-3 (Brown et al. 2020b)) or existing concept banks (e.g., ConceptNet (Speer, Chin, and Havasi 2017)). However, CBMs’ explanations are still restricted to pre-defined concepts, and they are not necessarily reliable because CBMs often predict the concepts without mapping to corresponding input regions (Huang et al. 2024). On the contrary, our XBMs directly generate natural language explanations to interpret the model outputs without pre-defined concepts.

Similar to our work, a few works attempted to generate linguistic explanations for target classification models (Hendricks et al. 2016; Nishida, Nishida, and Nishioka 2022). However, these methods require ground truth text explanations for training models, which are expensive and restrict applications. Our XBMs address this limitation by learning explanation generation by the classification loss and explanation distillation using a pre-trained text decoder.

## 5 Conclusion

In this paper, we presented a novel interpretable deep neural networks called explanation bottleneck models (XBMs). By leveraging pre-trained vision-language models, XBMs generate explanations corresponding to input and output in the forms of natural language description, concept phrases with contribution scores, and cross-attention heatmaps on input spaces. To ensure both the target task performance and the explanation quality, XBMs are optimized by the target task loss with explanation distillation, which penalizes the divergence between the distributions of the training and pre-trained text decoders. Experiments show that XBMs can achieve both high target task performance and accurate and fluent explanations; they achieve competitive performance to black-box baselines and largely outperform CBMs in target test accuracy. Furthermore, we found that training of XBMs can enhance the multi-modal understanding capability of backbone vision-language models even when using large vision-language models pre-trained on massive image-text pairs. We believe that this work introduces a new perspective on natural language explanations and advances the study of interpretable deep models to the next paradigm.

## Appendix

### A Detailed Setting

#### A.1 Training

We trained the models by the AdamW (Loshchilov and Hutter 2019) optimizer with the initial learning rate of  $3.0 \times 10^{-5}$  that decayed by cosine annealing. The training epochs were 100 on the Aircraft/Bird/Car datasets and 5 on the ImageNet dataset. We used mini-batch sizes of 32. The input samples were resized into resolutions of  $384 \times 384$  for XBM-BLIP and  $336 \times 336$  for XBM-LLaVA according to the setting of vision encoders. We used  $\lambda$  of 0.1 and  $\tau$  of 10 with exponential annealing by  $r_a = 1.0 \times 10^{-4}$  if not otherwise noted; we discuss the effect of  $\lambda$  and  $\tau$  in Section E. For the experiments on XBM-LLaVA, we fine-tuned the LoRA adapter parameters (Hu et al. 2022) of backbone language models instead of the entire parameters. We selected the final model by checking the validation accuracy for each epoch. We implemented the training and evaluation with PyTorch-1.13. We ran the experiments three times on a 24-core Intel Xeon CPU with eight NVIDIA A100 GPUs with 80GB VRAM and recorded the average evaluated on the final models; we omit the standard deviations for saving spaces, but we have confirmed the statistical significance of our method with a p-value  $< 0.05$  toward baselines.

#### A.2 Datasets

**ImageNet** (Russakovsky et al. 2015): We downloaded ImageNet from the official site <https://www.image-net.org/>. ImageNet is released under a license that allows it to be used for non-commercial research/educational purposes (see <https://image-net.org/download.php>).

**Aircraft (FGVC Aircraft)** (Maji et al. 2013): We downloaded FGVC Aircraft from the official site <https://www.robots.ox.ac.uk/~vgg/data/fgvc-aircraft/>. FGVC Aircraft is released under a license that allows it to be used for non-commercial research/educational purposes (see <https://www.robots.ox.ac.uk/~vgg/data/fgvc-aircraft/>).

**Bird (CUB-200-2011)** (Welinder et al. 2010): We downloaded CUB-200-2011 from the official site [http://www.vision.caltech.edu/datasets/cub\\_200\\_2011/](http://www.vision.caltech.edu/datasets/cub_200_2011/). CUB-200-2011 is released under a license that allows it to be used for non-commercial purposes (see <https://authors.library.caltech.edu/27452/>).

**Car (Stanford Cars)** (Krause et al. 2013): We downloaded Stanford Cars from the official site [https://ai.stanford.edu/~jkrause/cars/car\\_dataset.html](https://ai.stanford.edu/~jkrause/cars/car_dataset.html). StanfordCars is released under a license that allows it to be used for non-commercial research purposes (see [https://ai.stanford.edu/~jkrause/cars/car\\_dataset.html](https://ai.stanford.edu/~jkrause/cars/car_dataset.html)).

### B Additional Qualitative Experiments

Table 6 shows the qualitative evaluation results on the Aircraft and Car datasets, which are omitted in the main paper due to the page constraint. The evaluation protocol is the same as Section 3.2. Similar to Table 2, our method succeeded in capturing the semantic concepts of input images

in the text explanation. Also, the concept phrases and cross-attention heatmaps show that the captured semantic concepts contribute to the final output and the main focus of models is on the target objects.

### C Additional Results with Large Vision-Language Models

In Sections 3.3 and 3.4, we confirm the results of XBMs combined with LLaVA (XBM-LLaVA) on ImageNet. Here, we show the additional XBM-LLaVA results on the other datasets. Table 7 demonstrates the results with the same tendency as Table 3, i.e., combining XBMs with larger vision-language backbones significantly improves the target task performance and interoperability. This indicates that our methods can be extendable even if a new and powerful vision-language model emerges.

### D Additional Results of ImageNet Segmentation

We additionally compare our method with existing attribution methods on BLIP-ViT. Note that we omit this result from the main paper because, strictly speaking, BLIP-ViT and XBM-BLIP are different models and thus this evaluation is not a direct comparison. By following Chefer et al. (Chefer, Gur, and Wolf 2021), we tried LRP (Binder et al. 2016), partial-LRP (Voita et al. 2019), rollout (Abnar and Zuidema 2020), raw attention output from BLIP-ViT, GradCAM (Selvaraju et al. 2017), and the method of (Chefer, Gur, and Wolf 2021). Table 8 shows the results of ImageNet Segmentation with the same setting of Table 4. Surprisingly, the cross-attention output of the classifier  $f_\theta$  (i.e., Pre-trained BLIP and XBM-BLIP) significantly outperformed the conventional visualization methods in the segmentation metric. This indicates that visualization explanation outputs of XBMs are quite accurate and reliable as the interpretation of model outputs.

### E Detailed Analysis



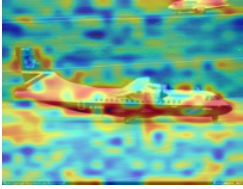
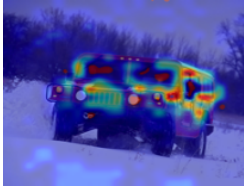
In this section, we provide detailed analyses of XBMs. In particular, we assess temperature annealing in the Gumbel softmax sampling (Eq. (6)), the hyperparameter  $\lambda$  in Eq. (1), and the localization ability of the cross-attention heatmaps introduced in Section 2.4.

#### E.1 Evaluations of Temperature Annealing

We introduce the temperature annealing strategy for determining  $\tau$  in Eq. (6). Here, we evaluate the effects by varying the initial temperature  $\tau^{(0)}$  in  $\{1, 10, 100\}$ . Table 9 shows the test performance and interpretability scores. We tested the cases leveraging a constant temperature  $\tau^{(0)}$  and applying exponential temperature annealing, i.e., + Annealing. In the cases of constant temperatures, we confirm that the larger temperatures tend to achieve better target performance but degrade perplexity scores. This is because using a larger temperature increases the entropy of the generative distribution of tokens in the Gumbel softmax sampling, and thus, it slightly loses the naturalness of the generated sentences. On the other



Table 6: Qualitative evaluation of explanation outputs.

	Aircraft (ATR-42)	Car (Hummer)
		
Pre-trained BLIP (Caption)	These two planes are parked on the tarmac at an airport run way.	Someone is driving a red jeep on a snowy road with trees in the background.
Label-free CBMs (Top-3 Concept)	canard foreplanes (0.70) a single-engine propeller (0.64) fixed landing gear (0.58)	2500HD model designation (0.63) off-road tires (0.40) distinct Suzuki grille (0.39)
XBMs (Text Explanation)	A small white and blue airplane on a runway at an airport with another plane in the background.	A truck with off-road tires driving through the snow in the wintertime with trees in the background.
XBMs (Top-3 Concept Phrase)	another plane in the background (0.34) a small white and blue airplane (0.31) a runway at an airport (0.22)	a truck with off-road tires (0.36) trees in the background (0.26) the wintertime (0.23)
XBMs (Cross-Attn. Heatmap)		

hand, applying the temperature annealing improved all scores in all initial temperatures. This implies that, by gradually reducing the temperature, XBMs can try to generate diverse tokens in the early stages of learning, and it narrows down only vocabulary with high likelihood in the later stages while the sentence naturalness is maintained.

## E.2 Effects of Hyperparameter $\lambda$

The hyperparameter  $\lambda$  in Eq (1) balances the target task training and the regularization to avoid the collapse of text explanations. Table 10 shows the results when varying  $\lambda$ . It demonstrates that the cases of  $\lambda > 0$  can avoid the collapse of the interpretability and improve target performance. We see that there is a trade-off between the target test accuracy and the GPT-2 Perplexity scores. In contrast, fortunately, CLIP-Score was less sensitive to the value of  $\lambda > 0$ , suggesting high-performance XBMs can still generate explanations well-related to inputs. Therefore, we recommend determining  $\lambda$  based on whether fluency or accuracy is a priority according to the application’s requirements.

## E.3 Explanation Distillation vs. Other Regularization

Here, we evaluate our explanation distillation regularization  $\mathcal{R}_{\text{int}}$  through a comparison to another regularization method. We compare our explanation distillation to L2SP (Li, Grandvalet, and Davoine 2018), which penalizes the model parameters by minimizing the l2 distance from the pre-trained parameters. Table 11 shows the results on the Car dataset. We

confirm that our explanation distillation outperforms L2SP in all performance metrics. Our method largely improves clip score, while L2SP degrades it from frozen BLIP. These results suggest that directly regularizing the decoder’s output helps XBMs explore the vocabulary needed for a task through classification loss while preserving natural sentences and minimizing the gap in the parameter space, which is harmful to this purpose.

## F Broader Impacts

A potential negative effect introduced by our work is that XBMs may output biased explanations if the backbone language model is extremely biased. This can be avoided by purifying the language model with existing debiasing methods such as (Kaneko and Bollegala 2021) before training XBMs. Since the target tasks handled by XBMs are no different from those in general models, off-the-shelf defence methods may be directly applicable to other risks such as adversarial attacks.

Table 7: Evaluation of XBMs with large vision-language models

<i>Aircraft</i>	Text Classifier $f_{\theta}(e)$			Multi-modal Classifier $f_{\theta}(h_{\psi}(x), e)$		
	Test Acc. ( $\uparrow$ )	CLIP-Score ( $\uparrow$ )	GPT-2 Perplexity ( $\downarrow$ )	Test Acc. ( $\uparrow$ )	CLIP-Score ( $\uparrow$ )	GPT-2 Perplexity ( $\downarrow$ )
Frozen BLIP	3.95	0.6824	155.8	45.23	0.6824	155.8
XBM-BLIP	24.36	0.7084	145.9	74.09	0.7151	129.8
Frozen LLaVA-v1.5-LLaMA-7B	59.21	0.7500	227.4	73.03	0.7514	227.3
XBM-LLaVA-v1.5-LLaMA-7B	64.11	0.7515	179.5	78.77	0.7595	184.8
XBM-LLaVA-v1.6-Vicuna-7B	68.64	0.7842	22.9	82.08	0.7758	34.7
XBM-LLaVA-v1.6-Mistral-7B	67.06	0.7769	39.9	81.55	0.7851	21.9
<i>Bird</i>	Text Classifier $f_{\theta}(e)$			Multi-modal Classifier $f_{\theta}(h_{\psi}(x), e)$		
	Test Acc. ( $\uparrow$ )	CLIP-Score ( $\uparrow$ )	GPT-2 Perplexity ( $\downarrow$ )	Test Acc. ( $\uparrow$ )	CLIP-Score ( $\uparrow$ )	GPT-2 Perplexity ( $\downarrow$ )
Frozen BLIP	5.53	0.7535	173.5	68.03	0.7535	173.5
XBM-BLIP	19.52	0.7910	168.5	80.99	0.7942	166.9
Frozen LLaVA-v1.5-LLaMA-7B	75.20	0.7788	140.8	75.67	0.7788	107.3
XBM-LLaVA-v1.5-LLaMA-7B	80.87	0.7981	107.3	83.07	0.8037	21.8
XBM-LLaVA-v1.6-Vicuna-7B	82.33	0.8130	21.0	84.93	0.8154	21.6
XBM-LLaVA-v1.6-Mistral-7B	81.53	0.8101	16.7	84.73	0.8110	16.7
<i>Car</i>	Text Classifier $f_{\theta}(e)$			Multi-modal Classifier $f_{\theta}(h_{\psi}(x), e)$		
	Test Acc. ( $\uparrow$ )	CLIP-Score ( $\uparrow$ )	GPT-2 Perplexity ( $\downarrow$ )	Test Acc. ( $\uparrow$ )	CLIP-Score ( $\uparrow$ )	GPT-2 Perplexity ( $\downarrow$ )
Frozen BLIP	7.98	0.6091	168.8	77.91	0.6091	168.8
XBM-BLIP	27.57	0.7127	168.5	89.47	0.7173	131.8
Frozen LLaVA-v1.5-LLaMA-7B	83.50	0.7236	99.8	91.19	0.7300	97.2
XBM-LLaVA-v1.5-LLaMA-7B	86.18	0.7300	97.2	92.82	0.7322	83.8
XBM-LLaVA-v1.6-Vicuna-7B	86.70	0.8081	35.7	93.85	0.8032	41.4
XBM-LLaVA-v1.6-Mistral-7B	86.75	0.8086	25.8	92.41	0.8071	27.9

Table 8: Evaluation of cross-attention map of XBMs on ImageNet Segmentation.

	Pixel Acc. ( $\uparrow$ )	mIoU ( $\uparrow$ )	mAP ( $\uparrow$ )
LRP (Binder et al. 2016)(BLIP-ViT)	46.25	29.69	48.51
partial-LRP (Voita et al. 2019) (BLIP-ViT)	53.59	36.29	65.06
rollout (Abnar and Zuidema 2020) (BLIP-ViT)	52.73	35.81	66.78
Raw Attention (BLIP-ViT)	57.12	39.00	67.92
GradCAM (Selvaraju et al. 2017) (BLIP-ViT)	61.84	39.68	63.48
Chefer et al. (Chefer, Gur, and Wolf 2021) (BLIP-ViT)	59.92	42.30	69.51
XBM-BLIP w/ Fixed Decoder	78.67	57.90	79.72
XBM-BLIP	80.90	60.80	80.18

## References

Abnar, S.; and Zuidema, W. 2020. Quantifying Attention Flow in Transformers. In *Annual Meeting of the Association for Computational Linguistics*.

Binder, A.; Montavon, G.; Lapuschkin, S.; Müller, K.-R.; and Samek, W. 2016. Layer-wise relevance propagation for neural networks with local renormalization layers. In *International Conference on Artificial Neural Networks*. Springer.

Brown, T.; Mann, B.; Ryder, N.; Subbiah, M.; Kaplan, J. D.; Dhariwal, P.; Neelakantan, A.; Shyam, P.; Sastry, G.; Askell, A.; Agarwal, S.; Herbert-Voss, A.; Krueger, G.; Henighan, T.; Child, R.; Ramesh, A.; Ziegler, D.; Wu, J.; Winter, C.; Hesse, C.; Chen, M.; Sigler, E.; Litwin, M.; Gray, S.; Chess, B.; Clark, J.; Berner, C.; McCandlish, S.; Radford, A.; Sutskever, I.; and Amodei, D. 2020a. Language Models are Few-Shot Learners. In *Advances in Neural Information Processing Systems*.

Brown, T.; Mann, B.; Ryder, N.; Subbiah, M.; Kaplan, J. D.;

Dhariwal, P.; Neelakantan, A.; Shyam, P.; Sastry, G.; Askell, A.; et al. 2020b. Language models are few-shot learners. *Advances in neural information processing systems*.

Chan, D.; Petryk, S.; Gonzalez, J.; Darrell, T.; and Canny, J. 2023. CLAIR: Evaluating Image Captions with Large Language Models. In *Proceedings of the 2023 Conference on Empirical Methods in Natural Language Processing*.

Chauhan, K.; Tiwari, R.; Freyberg, J.; Shenoy, P.; and Dvijotham, K. 2023. Interactive concept bottleneck models. In *Proceedings of the AAAI Conference on Artificial Intelligence*, volume 37, 5948–5955.

Chefer, H.; Gur, S.; and Wolf, L. 2021. Transformer interpretability beyond attention visualization. In *Proceedings of the IEEE/CVF conference on computer vision and pattern recognition*, 782–791.

Chiang, W.-L.; Li, Z.; Lin, Z.; Sheng, Y.; Wu, Z.; Zhang, H.; Zheng, L.; Zhuang, S.; Zhuang, Y.; Gonzalez, J. E.; Stoica,

Table 9: Effects of temperature  $\tau$  and annealing for Gumbel softmax sampling of XBMs (Car).

	Test Acc. ( $\uparrow$ )	CLIP-Score ( $\uparrow$ )	GPT-2 Perplexity ( $\downarrow$ )
$\tau^{(0)} = 1$	86.60	0.7138	140.8
+ Annealing	87.12	0.7258	127.3
$\tau^{(0)} = 10$	86.71	0.7148	143.9
+ Annealing	88.65	0.7253	133.0
$\tau^{(0)} = 100$	88.03	0.7168	146.2
+ Annealing	88.56	0.7272	143.6

Table 10: Effects of hyperparameter  $\lambda$  of XBMs (Car).

	Test Acc. ( $\uparrow$ )	CLIP-Score ( $\uparrow$ )	GPT-2 Perplexity ( $\downarrow$ )
$\lambda = 0$	86.59	0.4792	415.3
$\lambda = 0.01$	89.18	0.7158	163.4
$\lambda = 0.1$	89.47	0.7172	145.4
$\lambda = 0.3$	89.09	0.7148	138.9
$\lambda = 0.5$	88.62	0.7167	132.6
$\lambda = 0.7$	87.58	0.7158	131.7
$\lambda = 1.0$	87.59	0.7138	127.3

I.; and Xing, E. P. 2023. Vicuna: An Open-Source Chatbot Impressing GPT-4 with 90%\* ChatGPT Quality.

Devlin, J.; Chang, M.-W.; Lee, K.; and Toutanova, K. 2019. BERT: Pre-training of Deep Bidirectional Transformers for Language Understanding. In *Conference of the North American Chapter of the Association for Computational Linguistics*.

Dosovitskiy, A.; Beyer, L.; Kolesnikov, A.; Weissenborn, D.; Zhai, X.; Unterthiner, T.; Dehghani, M.; Minderer, M.; Heigold, G.; Gelly, S.; Uszkoreit, J.; and Houlsby, N. 2021. An Image is Worth 16x16 Words: Transformers for Image Recognition at Scale. In *International Conference on Learning Representations*.

Feng, W.; He, X.; Fu, T.-J.; Jampani, V.; Akula, A. R.; Narayana, P.; Basu, S.; Wang, X. E.; and Wang, W. Y. 2022. Training-Free Structured Diffusion Guidance for Compositional Text-to-Image Synthesis. In *The Eleventh International Conference on Learning Representations*.

Gandelsman, Y.; Efros, A. A.; and Steinhart, J. 2024. Interpreting CLIP’s Image Representation via Text-Based Decomposition. In *International Conference on Learning Representations*.

Guillaumin, M.; Küttel, D.; and Ferrari, V. 2014. Imagenet auto-annotation with segmentation propagation. *International Journal of Computer Vision*, 110: 328–348.

Hendricks, L. A.; Akata, Z.; Rohrbach, M.; Donahue, J.; Schiele, B.; and Darrell, T. 2016. Generating visual explanations. In *Proceedings of the European Conference on Computer Vision*.

Hessel, J.; Holtzman, A.; Forbes, M.; Le Bras, R.; and Choi, Y. 2021. CLIPScore: A Reference-free Evaluation Metric for Image Captioning. In *Proceedings of the 2021 Conference on Empirical Methods in Natural Language Processing*, 7514–7528.

Hinton, G.; Vinyals, O.; and Dean, J. 2015. Distilling the knowledge in a neural network. *arXiv preprint arXiv:1503.02531*.

Hu, E. J.; Shen, Y.; Wallis, P.; Allen-Zhu, Z.; Li, Y.; Wang, S.; Wang, L.; and Chen, W. 2022. LoRA: Low-Rank Adaptation of Large Language Models. In *International Conference on Learning Representations*.

Huang, Q.; Song, J.; Hu, J.; Zhang, H.; Wang, Y.; and Song, M. 2024. On the Concept Trustworthiness in Concept Bottleneck Models. In *Proceedings of the AAAI Conference on Artificial Intelligence*, volume 38, 21161–21168.

Jang, E.; Gu, S.; and Poole, B. 2017. Categorical reparameterization with gumbel-softmax. In *International Conference on Learning Representation*.

Jiang, A.; Sablayrolles, A.; Mensch, A.; Bamford, C.; Chaplot, D.; de las Casas, D.; Bressand, F.; Lengyel, G.; Lample, G.; Saulnier, L.; et al. 2023. Mistral 7B (2023). *arXiv preprint arXiv:2310.06825*.

Kaneko, M.; and Bollegala, D. 2021. Debiasing Pre-trained Contextualised Embeddings. In *Proceedings of the 16th Conference of the European Chapter of the Association for Computational Linguistics: Main Volume*, 1256–1266.

Kim, B.; Wattenberg, M.; Gilmer, J.; Cai, C.; Wexler, J.; Viegas, F.; et al. 2018. Interpretability beyond feature attribution: Quantitative testing with concept activation vectors (tcav). In *International conference on machine learning*.

Kim, Y.; and Rush, A. M. 2016. Sequence-Level Knowledge Distillation. In *Proceedings of the 2016 Conference on Empirical Methods in Natural Language Processing*. Association for Computational Linguistics.

Koh, P. W.; Nguyen, T.; Tang, Y. S.; Musmann, S.; Pierson, E.; Kim, B.; and Liang, P. 2020. Concept bottleneck models. In *International conference on machine learning*.

Table 11: Effects of Regularization in XBMs (Car).

	Test Acc. ( $\uparrow$ )	CLIP-Score ( $\uparrow$ )	GPT-2 Perplexity ( $\downarrow$ )
Frozen BLIP	77.91	0.6091	168.8
Explanation Distillation (Ours)	90.48	0.7173	131.8
L2SP (Li, Grandvalet, and Davoine 2018)	87.47	0.5059	159.4

Krause, J.; Stark, M.; Deng, J.; and Fei-Fei, L. 2013. 3D Object Representations for Fine-Grained Categorization. In *4th International IEEE Workshop on 3D Representation and Recognition*. Sydney, Australia.

Li, J.; Li, D.; Savarese, S.; and Hoi, S. 2023. Blip-2: Bootstrapping language-image pre-training with frozen image encoders and large language models. In *International conference on machine learning*.

Li, J.; Li, D.; Xiong, C.; and Hoi, S. 2022. Blip: Bootstrapping language-image pre-training for unified vision-language understanding and generation. In *International conference on machine learning*.

Li, X.; Grandvalet, Y.; and Davoine, F. 2018. Explicit inductive bias for transfer learning with convolutional networks. In *International Conference on Machine Learning*.

Liu, H.; Li, C.; Wu, Q.; and Lee, Y. J. 2023. Visual Instruction Tuning. In *Advances in Neural Information Processing Systems*.

Loshchilov, I.; and Hutter, F. 2019. Decoupled weight decay regularization. In *International Conference on Learning Representations*.

Maji, S.; Kannala, J.; Rahtu, E.; Blaschko, M.; and Vedaldi, A. 2013. Fine-Grained Visual Classification of Aircraft. *arXiv*.

Moayeri, M.; Rezaei, K.; Sanjabi, M.; and Feizi, S. 2023. Text-to-concept (and back) via cross-model alignment. In *International Conference on Machine Learning*.

Nishida, K.; Nishida, K.; and Nishioka, S. 2022. Improving Few-Shot Image Classification Using Machine- and User-Generated Natural Language Descriptions. In *Findings of the Association for Computational Linguistics: NAACL 2022*, 1421–1430.

Oikarinen, T.; Das, S.; Nguyen, L. M.; and Weng, T.-W. 2023. Label-free Concept Bottleneck Models. In *International Conference on Learning Representations*.

Radford, A.; Kim, J. W.; Hallacy, C.; Ramesh, A.; Goh, G.; Agarwal, S.; Sastry, G.; Askell, A.; Mishkin, P.; Clark, J.; et al. 2021. Learning transferable visual models from natural language supervision. In *International conference on machine learning*. PMLR.

Radford, A.; Wu, J.; Child, R.; Luan, D.; Amodei, D.; and Sutskever, I. 2019. Language Models are Unsupervised Multitask Learners.

Ramaswamy, V. V.; Kim, S. S.; Fong, R.; and Russakovsky, O. 2023. Overlooked factors in concept-based explanations: Dataset choice, concept learnability, and human capability. In *Proceedings of the IEEE/CVF Conference on Computer Vision and Pattern Recognition*.

Reed, S.; Akata, Z.; Lee, H.; and Schiele, B. 2016. Learning deep representations of fine-grained visual descriptions. In *Proceedings of the IEEE conference on computer vision and pattern recognition*.

Russakovsky, O.; Deng, J.; Su, H.; Krause, J.; Satheesh, S.; Ma, S.; Huang, Z.; Karpathy, A.; Khosla, A.; Bernstein, M.; et al. 2015. Imagenet large scale visual recognition challenge. *International Journal of Computer Vision*, 115(3).

Selvaraju, R. R.; Cogswell, M.; Das, A.; Vedantam, R.; Parikh, D.; and Batra, D. 2017. Grad-cam: Visual explanations from deep networks via gradient-based localization. In *Proceedings of the IEEE international conference on computer vision*, 618–626.

Speer, R.; Chin, J.; and Havasi, C. 2017. ConceptNet 5.5: An Open Multilingual Graph of General Knowledge. In *Proceedings of the AAAI Conference on Artificial Intelligence*.

Touvron, H.; Martin, L.; Stone, K.; Albert, P.; Almahairi, A.; Babaei, Y.; Bashlykov, N.; Batra, S.; Bhargava, P.; Bhosale, S.; et al. 2023. Llama 2: Open foundation and fine-tuned chat models. *arXiv preprint arXiv:2307.09288*.

Voita, E.; Talbot, D.; Moiseev, F.; Sennrich, R.; and Titov, I. 2019. Analyzing Multi-Head Self-Attention: Specialized Heads Do the Heavy Lifting, the Rest Can Be Pruned. In *Annual Meeting of the Association for Computational Linguistics*.

Welinder, P.; Branson, S.; Mita, T.; Wah, C.; Schroff, F.; Belongie, S.; and Perona, P. 2010. Caltech-UCSD Birds 200. Technical report, California Institute of Technology.

Wolf, T.; Debut, L.; Sanh, V.; Chaumond, J.; Delangue, C.; Moi, A.; Cistac, P.; Rault, T.; Louf, R.; Funtowicz, M.; et al. 2019. Huggingface’s transformers: State-of-the-art natural language processing. *arXiv preprint arXiv:1910.03771*.

Xu, X.; Qin, Y.; Mi, L.; Wang, H.; and Li, X. 2024. Energy-based concept bottleneck models: unifying prediction, concept intervention, and conditional interpretations. In *International Conference on Learning Representations*.

Yang, Y.; Panagopoulou, A.; Zhou, S.; Jin, D.; Callison-Burch, C.; and Yatskar, M. 2023. Language in a bottle: Language model guided concept bottlenecks for interpretable image classification. In *Proceedings of the IEEE/CVF Conference on Computer Vision and Pattern Recognition*.

Yuksekgonul, M.; Wang, M.; and Zou, J. 2023. Post-hoc Concept Bottleneck Models. In *International Conference on Learning Representations*.

Zarlenga, M. E.; Barbiero, P.; Ciravegna, G.; Marra, G.; Giannini, F.; Diligenti, M.; Precioso, F.; Melacci, S.; Weller, A.; Lio, P.; et al. 2022. Concept embedding models. In *Advances in Neural Information Processing Systems*.

Zhang\*, T.; Kishore\*, V.; Wu\*, F.; Weinberger, K. Q.; and Artzi, Y. 2020. BERTScore: Evaluating Text Generation with BERT. In *International Conference on Learning Representations*.

Zhou, B.; Khosla, A.; Lapedriza, A.; Oliva, A.; and Torralba, A. 2016. Learning deep features for discriminative localization. In *Proceedings of the IEEE conference on computer vision and pattern recognition*.